Complex Behavior in the Formaldehyde−Sulfite Reaction

K. Kovacs, R. McIlwaine, K. Gannon, A. F. Taylor,* and S. K. Scott

School of Chemistry, University of Leeds, Leeds LS2 9JT, U.K.

Received: August 9, 2004; In Final Form: October 7, 2004

The formaldehyde−sulfite reaction is an example of an "acid-to-alkali" clock. It displays an induction period, during which the pH varies only slowly in time, followed by a reaction event, during which the pH increases rapidly by several units. When the reaction is performed in a closed (batch) reactor, the clock time is found to increase with a decrease in initial concentrations of formaldehyde and sulfite and an increase in the total initial concentration of S(IV). At long times, following the clock event, there is a slow decrease in pH. In an open (flow) reactor, bistability between a low-pH steady state (pH ∼ 6−8) and a high-pH steady state (pH ∼ 11) is observed. Additionally, we report the existence of sustained, small-amplitude oscillations in pH in this system. An extended kinetic mechanism reproduces the batch behavior but fails to account for the complex behavior observed in the flow reactor. Possible additional reaction steps are discussed.

Introduction

Systems which might display oscillations in pH in batch reactors are of considerable interest. To date, the only nonlinear responses observed in thermodynamically closed systems are clock type behavior or a few damped oscillations.[1] Sustained oscillations have been obtained in flow reactors.[2] Interest in systems displaying robust pH oscillations arises as such reactions might contribute to the development of biomimetic devices, such as microvalves for the periodic delivery of drugs,[3,4] when used in conjunction with pH-sensitive polymers. The feedback processes involved in pH oscillating reactions might also give insight into certain biological phenomena such as temperature compensation,[5] i.e., the ability of systems to maintain periodic cycles of constant length within a physiological temperature range.

In pH-regulated reactions, the nonlinear production of hydrogen ion is the driving force for the dynamical behavior observed. A model for the systematic design of pH-regulated oscillators has been published,[6] essentially consisting of an autocatalytic production of H^+ coupled with an H^+ consuming process. Systems involving the oxidation of S(IV) species,[7] arsenite,[8] or hydroxylamine[9] by halogenate oxidants (e.g., IO_3^-, BrO_3^-, ClO_3^-) or hydrogen peroxide have been used as the autocatalytic, positive feedback subsystem. Sources of proton consumption/negative feedback include reductants such as ferrocyanide,[10] manganese complexes,[11] enzymes,[12] or carbon-(IV) species.[13] In batch, these pH-regulated reactions generally display an induction period with a high pH, followed by a rapid (or damped (oligo) oscillatory) transition to a lower pH. In flow, they are capable of displaying sustained large-amplitude oscillations in pH.[14]

An alternative class of pH oscillators is that in which the nonlinear pH change is a consequence of the dynamical behavior, rather than a driving force for it. One such reaction is the Cu(II)-catalyzed reaction between thiosulfate ($S_2O_3^{2-}$) and peroxodisulfate ($S_2O_8^{2-}$) which displays small-amplitude oscillations in pH when performed in a flow reactor.[15] The key feedback in this system is the autocatalytic production of radical species $SO_4^{\bullet-}$ and $S_2O_3^{\bullet-}$.

The formaldehyde−sulfite reaction is a well-known pH clock reaction,[16] which, contrary to the batch behavior of the systems described above, displays an induction period during which the pH is low and a reaction event during which the pH rapidly increases. This reaction is particularly interesting from a dynamical point of view as there is no obvious feedback in the proposed reaction mechanism, and the clock behavior is thought to result from the consumption of an internal sulfite−bisulfite buffer by formaldehyde to produce the formaldehyde−sulfite adduct, hydroxymethanesulfonate (HMS).[17,18] The reaction is also highly relevant in atmospheric chemistry as the oxidation of S(IV) species occurs in cloud or fog water with dissolved formaldehyde to give HMS.[19] This process is thought to provide a route for the stabilization of S(IV) with respect to oxidation by H_2O_2, which proceeds rapidly to yield sulfuric acid. The addition of organic ligands to sulfur species is also believed to have an inhibitive effect on the iron-catalyzed autoxidation of S(IV) in atmospheric fog water.[20]

In this paper, we investigate the formaldehyde−sulfite reaction, to obtain additional insight into the nonlinear kinetics observed in sulfur-based reactions.[21] In agreement with previous work we find that, in batch, the induction period can be related to the rate-determining dehydration of methylene glycol and the consumption of the sulfite−bisulfite buffer. We also find that the induction period increases with decreasing sulfite and that the pH gradually decreases following the reaction event, which has not been previously reported. The reaction is examined in a flow reactor, and complex behavior is observed, including bistability between a low-pH steady state (pH ∼ 6−8) and a high-pH steady state (pH ∼ 11), small amplitude oscillations (high pH), and bistability between the low-pH steady state and oscillations. A revised model quantitatively reproduces the main batch results but additional steps are required in order to reproduce the complex behavior observed in flow. Possible feedback routes are suggested.

* To whom correspondence should be addressed. E-mail: annettet@chem.leeds.ac.uk.

10.1021/jp0464324 CCC: $30.25
Published on Web 12/14/2004

TABLE 1: Mechanism for the Formaldehyde−Sulfite Clock Reaction

reaction	rate constants (k_f; k_r)
(1) $CH_2(OH)_2 \rightleftharpoons CH_2O + H_2O$	5.5×10^{-3} s^{-1}; 10 s^{-1}
(2) $HSO_3^- \rightleftharpoons SO_3^{2-} + H^+$	3.1×10^3 s^{-1}; 5×10^{10} M^{-1} s^{-1}
(3) $CH_2O + SO_3^{2-} \rightarrow CH_2(O^-)SO_3^-$	5.4×10^6 M^{-1} s^{-1}
(4) $CH_2(O^-)SO_3^- + H^+ \rightleftharpoons CH_2(OH)SO_3^-$	1×10^9 M^{-1} s^{-1}; 2×10^{-3} s^{-1}
(5) $H_2O \rightleftharpoons H^+ + OH^-$	1×10^{-3} M s^{-1}; 1×10^{11} M^{-1} s^{-1}
(6) $CH_2O + HSO_3^- \rightarrow CH_2(OH)SO_3^-$	4.5×10^2 M^{-1} s^{-1}
(7) $CH_2(OH)_2 + SO_3^{2-} \rightarrow CH_2(O^-)SO_3^- + H_2O$	2.5 M^{-1} s^{-1}
(8) $CH_2(OH)_2 + HSO_3^- \rightarrow CH_2(OH)SO_3^- + H_2O$	0.48 M^{-1} s^{-1}

Experimental and Calculations

For both batch and flow reactions, two stock solutions were prepared using analytical grade chemicals and doubly distilled deionized water. Solution A contained methylene glycol (37% formalin solution, Aldrich) and the hydrated form of formaldehyde and was diluted to give the required concentration 24 h prior to use to allow complete de-polymerization.[22] Solution B contained sodium metabisulfite (Vickers) and sodium sulfite (Vickers). Sulfur species in solution B are prone to aerial oxidation, which results in a lengthening of the induction time. Since oxidation is catalyzed by transition metal ions, ethylenediaminetetraacetic acid (EDTA; 5×10^{-3} M; Vickers) was also added to the stock solution. Solution B was used directly after preparation in batch experiments and continuously bubbled with nitrogen during the flow experiments.

The batch experiments were carried out in a small (20 mL) reaction vessel containing a magnetic stirrer to ensure complete mixing on addition of solution A to solution B. Typical concentrations in stock solutions were as follows: A, $[CH_2(OH)_2]_0 = 1.2$ M; B, $[HSO_3^-]_0 = 0.2$ M and $[SO_3^-]_0 = 0.02$ M. The total volume of the reagents was always 10 mL, and the required volumes of stock solutions mixed with distilled water to give the concentrations stated in the text. The stock solutions were maintained at 22 °C. A calibrated pH electrode (HANNA) was used to accurately measure the pH as a function of time, in 1 s intervals. The induction time was determined from the digitized data via the second derivative of the pH−time plot. Additional experiments were performed in 1 M NaCl to ensure ionic strength had no significant influence on the induction time/pH change.

The flow experiments were performed in a continuously fed stirred tank reactor (CSTR) of volume 22 mL and completely filled to ensure there was no solution/air interface. The reactor was surrounded by a water jacket, and reactions were performed at constant temperature. The solution was stirred with a magnetic stirrer (500 rpm). The stock solutions were supplied to the reactor by use of a calibrated peristaltic pump (Gilson). pH and temperature were monitored using a HANNA pH electrode and digital meter.

Calculations

Simulations of experiments were performed using the mechanism in Table 1. This is an extended version of the model (steps 1−5) proposed by Boyce and Hoffmann.[23] The rate constants for steps 1−5 have been determined previously, and the rate constants for the new additional steps 6−8 were varied in this work to reproduce batch experimental results. Numerical integration of the eight resulting differential equations was performed using package XPPAUT.[24] The method of integration chosen was CVODE, with a time step generally taken as $dt = 0.01$ and the tolerance set at tol $= 1 \times 10^{-7}$.

Results

Batch Reactor. Typical pH vs time plots are shown in Figure 1a for the batch reaction of methylene glycol with the bisulfite−sulfite buffer. The initial concentrations were $[CH_2(OH)_2]_0 = 0.096$ M (0.192 stock) and $[HSO_3^-]_0 = 0.0631$ M (0.1262 stock), and the sulfite concentration was then varied between experiments. In each case there is an induction period t_{ind} during which the pH is increasing slowly, followed by a relatively rapid increase in pH. The initial pH is governed by ratio of bisulfite/sulfite through the rapid equilibrium in reaction 2. The induction period was of the order of tens of seconds and is observed to increase with decreasing initial concentration of sulfite. The increase in pH in the reaction event is between 4 and 5 units. The long-term behavior of the closed system demonstrates a subsequent gradual decrease in pH following the reaction event (Figure 1b).

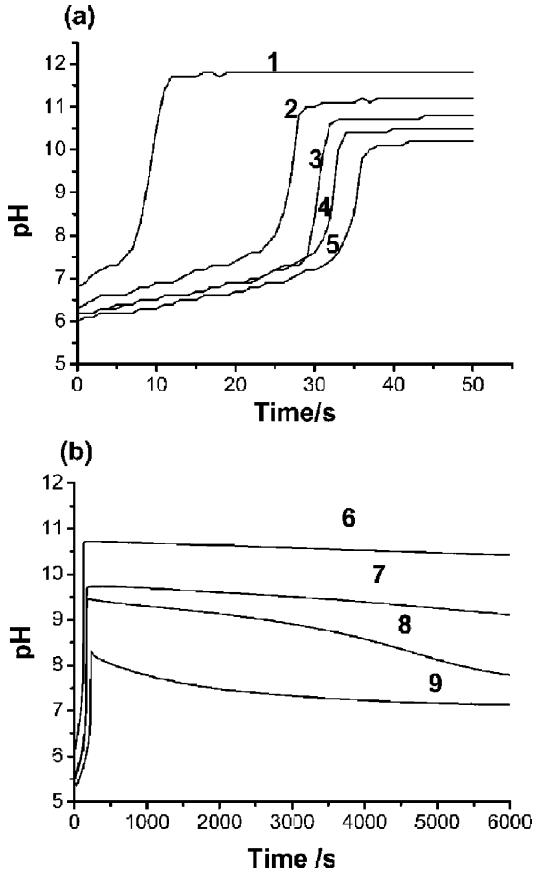

Figure 1. (a) Experimental pH time traces in the batch reactor with different initial sulfite concentrations. $[CH_2(OH)_2]_0 = 0.096$ M, $[HSO_3^-]_0 = 0.063$ M, and $b/c = 1$ (1), 5 (2), 8 (3), 10 (4), 15 (5). (b) Long time behavior in batch with different initial sulfite concentrations: $[CH_2(OH)_2]_0 = 0.025$ M, $[HSO_3^-]_0 = 0.0166$ M, and $b/c = 13$ (6), 57 (7), 117 (8), and with $[SO_3^{2-}]_0 = 0$ M (9).

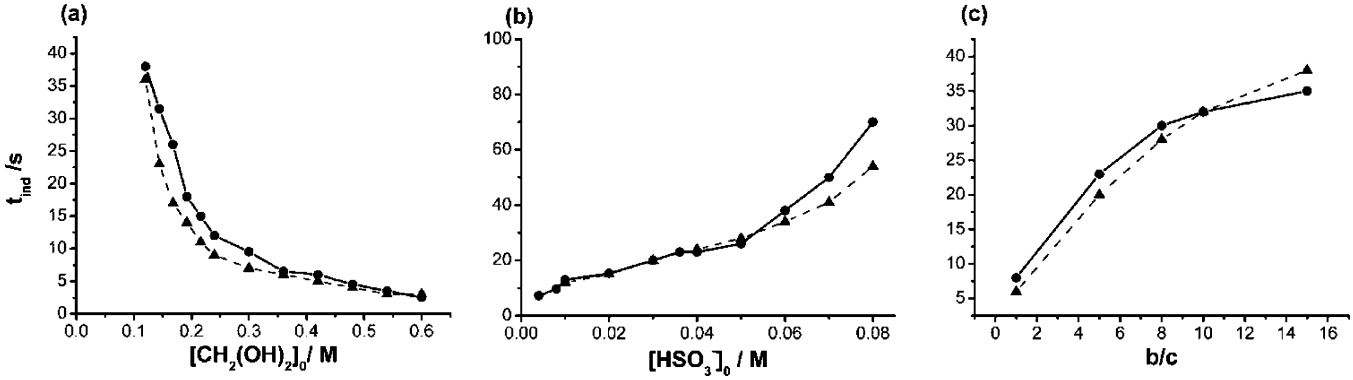

Figure 2. Experimental (●) and numerical (▲) variation of induction time with (a) $[CH_2(OH)_2]_0$, where $[HSO_3^-]_0 = 0.1$ M, $b/c = 10$; (b) $[HSO_3^-]_0$, where $b/c = 10$ and $[CH_2(OH)_2]_0 = 0.096$ M; and (c) $[SO_3^{2-}]_0$, where $[HSO_3^-] = 0.063$ and $[CH_2(OH)_2]_0 = 0.096$ M.

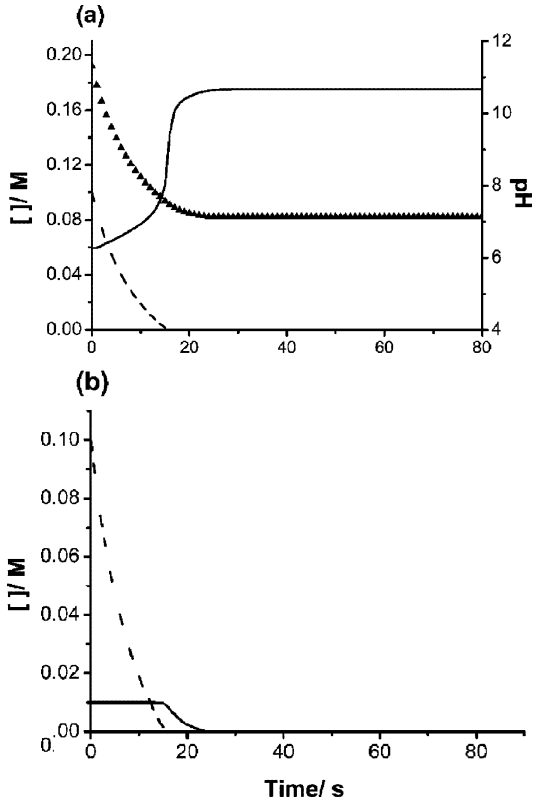

Figure 3. Computed variations in time of (a) pH (—), $[CH_2(OH)_2]$ (▲), and $[HSO_3^-]$ (--) and (b) $[HSO_3^-]$ (--) and $[SO_3^{2-}]$ (—). The initial species concentrations: $[CH_2(OH)_2]_0 = 0.192$ M, $[HSO_3^-]_0 = 0.1$ M, and $b/c = 10$.

The experimental variation of the induction period with the initial concentrations of (a) methlyene glycol, (b) total sulfur containing species keeping the ratio of bisulfite/sulfite (b/c) constant, and (c) sulfite is shown in Figure 2.

The calculated evolution of the concentrations of the main species is plotted in Figure 3 for a system with the initial composition $[CH_2(OH)_2]_0 = 0.192$ M and $[HSO_3^-]_0 = 0.1$; $b/c = 10$. During the induction period, the concentrations of $CH_2(OH)_2$ and HSO_3^- decrease and the pH increases, while that of SO_3^{2-} remains constant. The buffer equilibrium in step 2 is maintained during this period so $[SO_3^{2-}][H^+]/[HSO_3^-] = K_2 = 6.2 \times 10^{-8}$. This also implies that the ratio $[H^+]/[HSO_3^-]$ remains constant over this period, and the computations indicate that $[HSO_3^-]$ decreases exponentially (pseudo-first-order kinetics) and the pH increases linearly in time over the induction period. Once the bisulfite has been sufficiently consumed, a rapid increase in pH is observed and there is then decay in the concentration of sulfite. The computed variations of the induction period with initial species concentrations are compared with the experimental results in Figure 2. The induction period is sensitive to the rate coefficients for step 1 and steps 6−8, the qualitative dependence can be modeled successfully in each case, and suitable adjustments to the rate coefficients allow reasonable quantitative agreement.

Flow Reactor. Under flow conditions, this system is able to support bistability for a range of operating conditions. An example a bifurcation diagram for this response is shown in Figure 4a, where we see the coexistence of the low-pH flow branch and the high-pH thermodynamic branch at high flow rates. The "ignition" transition from the flow branch to the thermodynamic branch at low flow rates is clearly determined at a flow rate of ca. 23 mL min^{-1}. The corresponding "washout" transition occurs at too high a flow rate for us to locate this in our system, so we are unable to determine the full extent of the hysteresis region.

The form of the bifurcation diagram changes as the ratio of bisulfite to sulfite (elsewhere referred to as b/c) is varied, with the region of bistability decreasing as this ratio is increased. The response shown in Figure 4b again shows two branches at low and high pH, respectively, for a system with $b/c = 5$. However, the character of the upper branch changes as the flow rate is increased, and there is a Hopf bifurcation such that the high-pH steady state loses stability and a stable, small amplitude oscillatory state emerges. Thus, there are two different types of bistability evident in this diagram: BS2 indicates a region of coexistence of two stable steady states (as in Figure 4a) and BS1 indicates a region of coexistence of a stable steady state (low pH) and an oscillatory state (high pH).

A further example of an experimental bifurcation diagram is shown in Figure 5 for a system with $b/c = 116$. A high-pH oscillatory state exists at low flow rates (OSC), followed by bistability between two oscillatory states (BS3) for a small range of experimental conditions; in this case, a Hopf bifurcation also occurs on decreasing k_0, in the vicinity of the "ignition point" at the low-flow-rate end of the lower branch of solutions, and small-amplitude oscillatory states are observed. For a larger range of flow rates, a low-pH steady state and a high-pH oscillatory state coexist (BS2). An example time series of the high-pH oscillatory response at $k_0 = 2.81$ mL min^{-1} is shown in the inset to this figure, recorded by a Pt electrode and a pH electrode. The small-amplitude (0.4 pH units) and the long time constant on the pH electrode system employed generally produces "noisy" time series data, but these examples indicate that the waveform is essentially that of a simple, period-1 response. The variation of the amplitude of the oscillatory solution with flow rate is indicated in Figure 5 by the size of

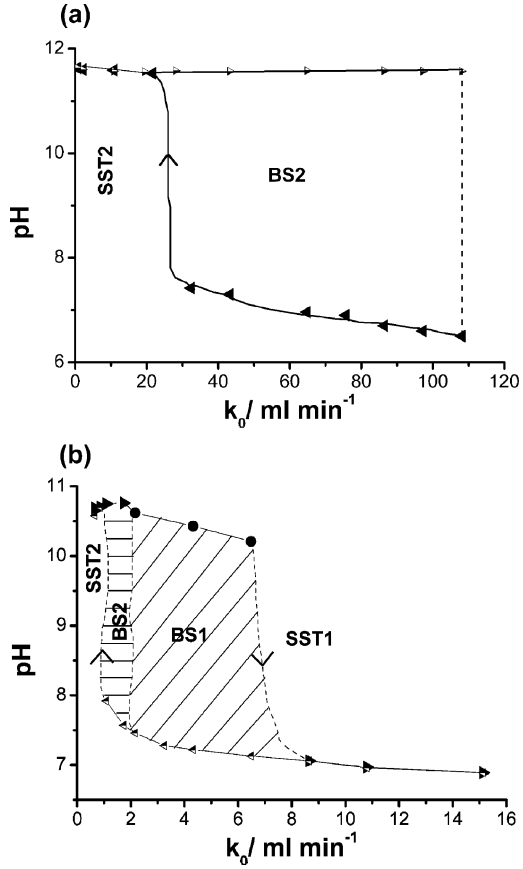

Figure 4. (a) Bifurcation diagram showing the regions of high-pH steady state (SST2) and bistability between two steady states (BS2), where $[CH_2(OH)_2]_0 = 0.17$ M, $[HSO_3^-]_0 = 0.1$ M, $[SO_3^{2-}]_0 = 0.01$ M, and $T = 22$ °C. (b) Bifurcation diagram showing the regions of high pH steady state (SST2), bistability between two steady states (BS2), bistability between the low-pH steady state and the oscillatory state (BS1), and low-pH steady state (SST1) where $[CH_2(OH)_2]_0 = 0.067$ M, $[HSO_3^-]_0 = 0.066$ M, $[SO_3^{2-}]_0 = 0.0133$ M, and $T = 22$ °C. (Filled triangles) steady state with increasing flow rate; (filled circles) oscillatory state with increasing flow rate, (triangles half-filled) steady state with decreasing flow rate.

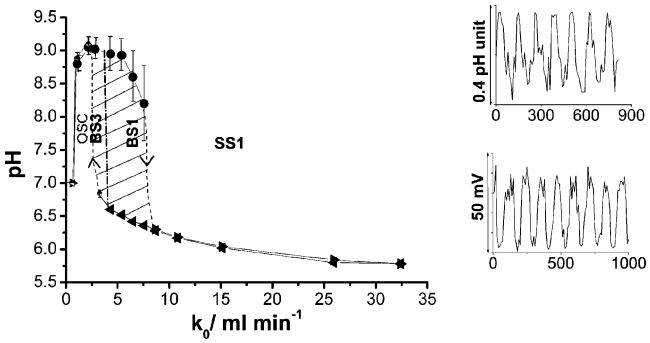

Figure 5. Bifurcation diagram showing the regions of thermodynamic steady state (pH ~ 7), high-pH oscillations (OSC), bistability between two oscillatory states (BS3), bistability between low-pH steady state and the oscillatory state (BS1), and the low-pH steady state (SS1), where $[CH_2(OH)_2]_0 = 0.089$ M, $[HSO_3^-]_0 = 0.066$ M, $[SO_3^{2-}]_0 = 5.7 \times 10^{-4}$ M, and $T = 22$ °C. (Filled circles) oscillatory state with increasing flow rate (the vertical lines show the amplitude of the oscillations); (half-filled circles) oscillatory state with decreasing flow rate, (filled triangles pointing right) steady state with increasing flow rate, and (filled triangles pointing left) steady state with decreasing flow rate. Oscillations are shown in pH (top left) and potential at $k_0 = 2.81$ mL min^{-1}.

the vertical "bars" superimposed on the upper branch. The amplitude increases with increasing flow rate, and the period

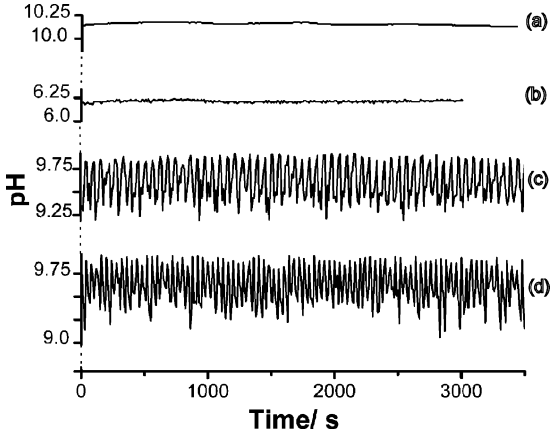

Figure 6. pH−time curves at different flow rates. (a) $[SO_3^{2-}] = 0.052$ M, T = 22 °C, $k_0 = 21.61$ mL min^{-1} (no reaction); (b) $[CH_2(OH)_2]_0 = 0.10$ M, $[HSO_3^-]_0 = 0.066$ M, $[SO_3^{2-}]_0 = 5.7 \times 10^{-4}$ M, T = 22 °C, $k_0 = 14.05$ mL min^{-1}; (c) $k_0 = 2.16$ mL min^{-1}; (d) $k_0 = 3.24$ mL min^{-1}.

decreases (from 40 to 30 s across the range in this particular bifurcation diagram).

Although the oscillatory amplitude is small in this system, ranging from 0.3 to 1 pH unit, it is distinguishable from the typical levels of noise in experimental time series. Time series for (a) sulfite-only solution at a high flow rate (21.6 mL min^{-1}) and (b) a low-pH steady-state at a flow rate of 14 mL min^{-1} shown in Figure 6 have noise levels of only 0.01 pH units. Example time series for genuine oscillatory states at lower flow rates are shown for comparison in Figure 6c,d.

The sustained oscillatory response is robust and observed over a wide range of operating conditions, including over a wide temperature range (4−53 °C). The different responses exhibited by this system are summarized in the k_0−$[HCHO]_0$ and k_0−(b/c) parameter planes in Figure 7a,b, respectively. These diagrams indicate the extent of the regions of different types of bistability, of unique steady states, and of oscillatory states.

Discussion

The behavior described above ranges from a detailed investigation of the previously known clock reaction in batch to the observation of bistability and oscillations under flow conditions. For clock reactions based on autocatalytic or self-inhibitory feedback, the link between clock in batch to bistability in a flow reactor is well-established and expected. A systematic methodology exists for "designing" oscillatory systems based on bistability, following the approach of Epstein et al.[25] in which an additional feedback process is added to the bistable system. In the present system, there are two surprises. First, bistability is observed even though there is no obvious autocatalysis in the mechanism, and second, oscillations are observed without the apparent requirement for a second feedback process. These experimental observations appear to be completely robust and repeatable but leave some unanswered questions with regard to the underlying mechanistic origins.

The mechanism of the formaldehyde-sulfite reaction has been developed over a number of previous studies over a range of pH conditions. Boyce and Hoffman[17] investigated the reaction under acidic conditions and, more recently, by Winkleman and Beenackers.[26] The latter authors adopt a mechanism similar to that of Boyce and Hoffman—steps1−5 in the model above—which adequately describes the observed clock-type behavior, provided the concentration of formaldehyde, which exists mainly in its hydrated form, is greater than that of bisulfite + sulfite.

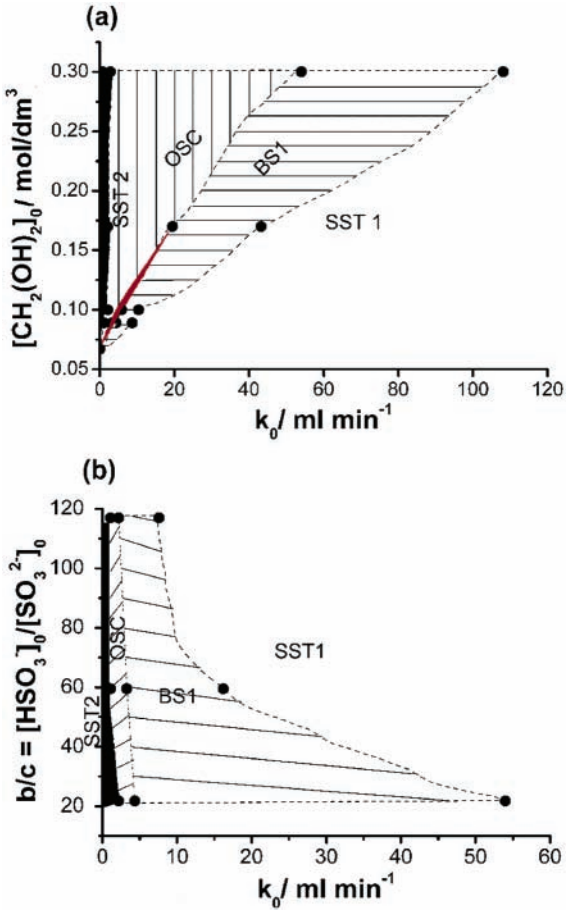

Figure 7. (a) $[CH_2(OH)_2]_0$−flow rate phase diagram showing the regions of high-pH steady state (black area, SST2), low-pH steady state (SS1), high-pH oscillatory state (OSC), bistability between the low-pH steady state and the high-pH oscillatory state (BS1), bistability between two oscillatory states (red area, BS3), where $[HSO_3^-]_0 = 0.066$ M, $[SO_3^{2-}]_0 = 5.7 \times 10^{-4}$ M, $T = 22$ °C. (b) $[HSO_3^-]/[SO_3^{2-}]$−flow rate phase diagram where $[CH_2(OH)_2]_0 = 0.089$ M, $[HSO_3^-]_0 = 0.066$ M, and $T = 22$ °C.

The rate-determining step is the dehydration of methlylene glycol, and the pH is determined by the internal bisulfite−sulfite buffer (reaction 2). As the reaction proceeds, SO_3^{2-} and H^+ are consumed through reactions 3 and 4, but are supplied through the dissociation of HSO_3^- in reaction 2, and the pH increases slowly. When HSO_3^- has been completely consumed, reaction 2 can no longer supply H^+ to match its consumption through reaction 4 and the pH increases rapidly.

The decrease in the induction period with increasing initial concentration of methylene glycol (Figure 2a) can be explained by the increase in the rate of reaction 1 and thus the rate of removal of SO_3^{2-}. The increase in induction period observed upon increasing the total concentration of sulfur containing species (Figure 2b) can be explained by the corresponding increase in the time for the total consumption of HSO_3^-. Reactions 1−5 reproduce these features qualitatively in simulations, but grossly overestimate the clock time. Reaction 6 has been proposed by Skrabal and Skrabal:[27] although this had been thought to be an insignificant reaction channel, the addition of this reaction has been important for modeling the behavior at low S(IV) concentrations.

From this description of the clock behavior, a decrease in the concentration of sulfite alone should result in a decrease in the induction time. However, we observed an increase in the induction time (Figure 1c), a feature which is not reproduced by reaction steps 1−6. The addition of reactions 7 and 8, proposed by Lagrange et al.,[28] provides additional S(IV)-consuming processes and can explain the experimental trends reported here. The values of the rate coefficients for these two steps, along with that for step 1, are mainly responsible for determining the computed induction periods.

The formaldehyde−sulfite clock reaction can thus be explained by the existence of a buffer which maintains the acidic pH until it is completely consumed. Although the rate of production of OH^- is acceleratory, the model does not contain any obvious feedback. This model, however, does not account for the complex behavior observed in flow, including bistability between steady states and oscillations. Simulations performed under flow conditions resulted in the observation of only a single steady state. To observe the high-pH steady state in flow, a feedback process is required which may be autocatalytic in OH^-, i.e., pH-regulated or autocatalytic in another species in a reaction step in which OH^- is produced. Nevertheless, it is well-understood that autocatalysis alone is not necessarily sufficient for the observation of oscillations in an open system, and additional negative feedback may be essential. Several feedback processes have been identified in related systems which may be pertinent to the work reported here. In basic solution, methylene glycol may undergo a Cannizzaro-type reaction, resulting in the formation of methanol and formic acid, and there is some evidence of a radical chain reaction occurring, although the generally accepted mechanism simply involves hydride transfer.[29] A related reaction is the condensation of formaldehyde in basic solution producing sugars (the Formose reaction), which has been reported to be autocatalytic in hydrated intermediates such as glycol−aldehyde. This reaction may display bistability when performed in an open reactor, but this is thought to result from insufficient observation times and no oscillations have been reported in this system.[30] Alternatively, the oxidation of S(IV) by gallic acid has recently been demonstrated to result in nonlinear production of S(VI). Self-inhibition of the production of an organic radical species was proposed to account for the observed nonlinearity.[20] The possibility of a similar feedback mechanism in the formaldehyde−sulfite reaction will be investigated in a subsequent paper.

Conclusion

The formaldehyde−sulfite reaction displays interesting nonlinear dynamical behavior. In batch, this reaction displays an induction period during which the pH is acidic followed by a rapid transition to an alkaline pH. This behavior can be explained by the existence of an internal buffer through HSO_3^- and SO_3^- which maintains an acidic pH until it is completely consumed and a transition to the high pH follows. In a flow reactor, bistability between steady states has been observed, but also pH oscillations and bistability between a low-pH steady state and oscillations. Further investigations are required to elucidate the additional reaction steps necessary to reproduce the complex behavior.

Acknowledgment. The authors acknowledge the support of EPSRC Grant No. GR/S47502/01 and Prof. Gy. Rabai and Prof. V. Gaspar (Debrecen) for helpful discussion, and R.M. thanks ESF REACTOR.

References and Notes

(1) Rabai, G. *J. Chem. Soc., Chem. Commun.* **1991**, *16*, 1083−1084.
(2) Rabai, G. *ACH−Models Chem.* **1998**, *135*, 381−392.
(3) Misra, G. P.; Siegel, R. A. *J. Controlled Release* **2002**, *79*, 293−297.

(4) Giannos, S. A.; Dinh, S. M.; Berner, B. *J. Pharm. Sci.* **1995**, *84*, 539−543.
(5) Kovacs, K. M.; Rabai, G. *Phys. Chem. Chem. Phys.* **2002**, *4*, 5265−5269.
(6) Luo, Y.; Epstein, I. R. *J. Am. Chem. Soc.* **1991**, *113*, 1518−1522.
(7) Frerichs, G. A.; Mlnarik, T. M.; Grun, R. J.; Thompson, R. C. *J. Phys. Chem. A* **2001**, *105*, 829−837.
(8) De Kepper, P.; Epstein, I.; Kustin, K. *J. Am. Chem. Soc.* **1981**, *103*, 2133−2134.
(9) Rabai, G.; Epstein, I. R. *J. Phys. Chem.* **1990**, *94*, 6361−6365.
(10) Rabai, G.; Kaminaga, A.; Hanazaki, I. *J. Phys. Chem.* **1996**, *100*, 16441−16442.
(11) Okazaki, N.; Rabai, G.; Hanazaki, I. *J. Phys. Chem. A* **1999**, *103*, 10915−10920.
(12) Hauser, M. J. B.; et al. *Faraday Discuss.* **2001**, *120*, 229−236.
(13) Rabai, G.; Hanazaki, I. *J. Phys. Chem.* **1996**, *100*, 10615−10619.
(14) Kovacs, K. M.; Rabai, G. *J. Phys. Chem. A* **2001**, *105*, 9183−9187.
(15) Orban, M.; Kurin-Csorgei, K.; Rabai, G.; Epstein, I. R. *Chem. Eng. Sci.* **2000**, *55*, 267−273.
(16) Warneck, P. *J. Chem. Educ.* **1989**, *66*, 334−335.
(17) Olson, T. M.; Boyce, S. D.; Hoffmann, M. R. *Prepr.—Am. Chem. Soc., Div. Pet. Chem.* **1986**, *31*, 546−550.
(18) Winkelman, J. G. M.; et al. *Chem. Eng. Sci.* **2002**, *57*, 4067−4076.
(19) Olson, T. M.; Hoffmann, M. R. *Atmos. Environ. (1967−1989)* **1989**, *23*, 985−997.
(20) Pasiuk-Bronikowska, W.; Bronikowski, T.; Ulejczyk, M. *J. Phys. Chem. A* **2003**, *107*, 1742−1748.
(21) Ojo, J. F.; Otoikhian, A.; Olojo, R.; Simoyi, R. H. *J. Phys. Chem. A* **2004**, *108*, 2457−2463.
(22) Burnett, M. G. *J. Chem. Educ.* **1982**, *59*, 160−162.
(23) Boyce, S. D.; Hoffmann, M. R. *J. Phys. Chem.* **1984**, *88*, 4740−4746.
(24) http://www.math.pitt.edu/∼bard/xpp/xpp.html.
(25) Epstein, I. R.; Kustin, K.; De Kepper, P.; Orban, M. *Sci. Am.* **1983**, *248*, 96.
(26) Winkleman, O.; Beenackers. *Chem. Eng. Sci.* **2000**, *55*, 2065.
(27) Skrabal, A.; Skrabal, R. *Monatsh. Chem.* **1936**, *69*, 11−41.
(28) Lagrange, J.; Wenger, G.; Lagrange, P. *J. Chim. Phys. Phys.-Chim. Biol.* **1999**, *96*, 610−633.
(29) Ashby, E. C.; Coleman, D.; Gamasa, M. *J. Org. Chem.* **1987**, *52*, 4079−4085.
(30) Huskey, W. P.; Epstein, I. R. *J. Am. Chem. Soc.* **1989**, *111*, 3185.